

# Towards a Quantum Hardware Roofline: Evaluating the Impact of Gate Expressivity on Processor Design

*Justin Kalloor  
Mathias Weiden  
Ed Younis  
De Jong Wibe  
John D. Kubiawicz  
Iancu Costin*

Electrical Engineering and Computer Sciences  
University of California, Berkeley

Technical Report No. UCB/EECS-2024-78

<http://www2.eecs.berkeley.edu/Pubs/TechRpts/2024/EECS-2024-78.html>

May 10, 2024



Copyright © 2024, by the author(s).  
All rights reserved.

Permission to make digital or hard copies of all or part of this work for personal or classroom use is granted without fee provided that copies are not made or distributed for profit or commercial advantage and that copies bear this notice and the full citation on the first page. To copy otherwise, to republish, to post on servers or to redistribute to lists, requires prior specific permission.

---

**Towards a Quantum Hardware Roofline: Evaluating the Impact of  
Gate Expressivity on Processor Design**

by Justin Kalloor

---

**Research Project**

Submitted to the Department of Electrical Engineering and Computer Sciences,  
University of California at Berkeley, in partial satisfaction of the requirements for the  
degree of **Master of Science, Plan II**.

Approval for the Report and Comprehensive Examination:

**Committee:**

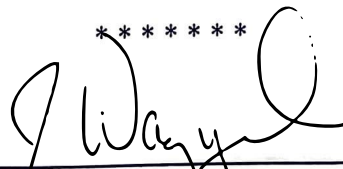


Professor John Kubiatoicz  
Research Advisor

5/7/24

May 7, 2024

\*\*\*\*\*



Professor John Wawrzynek  
Second Reader

## Abstract

The design space of current quantum computers is expansive, with no obvious winning solution, leaving practitioners with a crucial question: “What is the optimal system configuration to run an algorithm?” This paper explores hardware design trade-offs across NISQ systems to better guide algorithm and hardware development. Algorithmic workloads and fidelity models drive the evaluation to appropriately capture architectural features such as gate expressivity, fidelity, and crosstalk. As a result of our analysis, we extend the criteria for gate design and selection from only maximizing average fidelity to a more comprehensive approach that additionally considers expressivity with respect to algorithm structures. A custom synthesis-driven compilation workflow that produces minimal circuit representations for a given system configuration drives our methodology and allows us to analyze any gate set effectively. In this work, we focus on native entangling gates (CNOT, ECR, CZ, ZZ, XX, Sycamore,  $\sqrt{i}$ SWAP), proposed gates (B Gate,  $\sqrt[4]{\text{CNOT}}$ ,  $\sqrt[3]{\text{CNOT}}$ ), as well as parameterized gates (FSim, XY). By providing a method to evaluate the suitability of algorithms for hardware platforms, this work emphasizes the importance of hardware-software codesign for quantum computing.

## 1 Introduction

Quantum computers offer an exciting opportunity to explore problems previously considered intractable. An assortment of companies have introduced gate-based quantum machines that range in qubit technology: superconducting transmon qubits [5], fluxonium qubits [4], trapped-ion qubits [10], neutral atoms [23], and several others.

While existing hardware offerings are not mature enough to provide realistic quantum advantage [1] or quantum utility [24], they can be used as a good indicator of the future. Practical questions have already arisen in the community related to the comparison of different hardware solutions: “What computer should I use to run my algorithm? How can I improve my current quantum processor? What gates should I provide to end-users?”

In the current Noisy Intermediate Scale Quantum (NISQ) computing era, gates are imperfect and introduce error in program outputs. Thus, the most important performance metric for current systems is their ability to execute algorithms with the least amount of error, i.e. maximize algorithmic fidelity.

To this end, hardware designers attempt to improve the accuracy of an algorithm’s execution using a multi-stage design process aimed at optimizing behavior across multiple hardware characterization criteria: gate fidelity, crosstalk (gate parallelism and qubit connectivity), etc. This process, centered around gate fidelity, proceeds as follows: First choose a native entangling two-qubit gate that can be implemented with high fidelity, and that is “good enough” to represent any two qubit process (unitary). After this, develop additional techniques, e.g. crosstalk mitigation, to further improve gate fidelity.

We believe that this design process can be improved upon from both a hardware and end-user perspective. Most hardware characterization metrics

([30, 12, 25]) are gate and algorithm agnostic; therefore, these widely accepted metrics (e.g. gate fidelity) are hard to correlate directly with algorithm performance across systems with distinct hardware characteristics. Full algorithm fidelity models that capture hardware characteristics (gate fidelity and parallelism/crosstalk) have been introduced in the literature [9]. While they are able to assess the fidelity of an algorithm when executed on a single hardware configuration, these models still lack predictive power when varying architectural parameters. The problem stems from the fact that these metrics combine algorithm-agnostic hardware characterization metrics with metrics that characterize the program implementation and resource consumption (e.g. gate count, circuit depth), and implicitly the impact of the program generators and compilers.

In this paper we argue that gate set design should be driven by representational power in the context of a given algorithm or algorithmic workload. In order to attain the most resource efficient implementation, we use custom compilation workflows that combine traditional compilers, such as Cirq [15] or Tket [44], with circuit synthesis tools. Note that the inferences made in this paper could not be obtained without leveraging the BQSKit [49] circuit synthesis tools.

The evaluation is driven by a workload that contains several algorithms of wide interest, such as QFT, QAOA [18], TFIM models [43], Quantum Finance algorithms [19], and Quantum Machine Learning models [8]. For each algorithm we consider problem instances of increasing scale (qubit count) and generate the most resource efficient implementation for a given hardware configuration (gate set and qubit interconnect topology). We consider native entangling gates (CNOT, ECR, CZ, ZZ, XX, Sycamore,  $\sqrt{i}$ SWAP), proposed gates (B Gate,  $\sqrt[4]{\text{CNOT}}$ ,  $\sqrt[5]{\text{CNOT}}$ ), as well as parameterized gates (FSim, XY), together with several qubit interconnect topologies.

This paper makes the following contributions:

First, we introduce analytical models that combine hardware (gate fidelity, parallelism and qubit connectivity) and algorithm implementation (gate count, depth) characteristics to provide useful guidance for hardware and compiler designers, as well as system end-users. We introduce a comparative performance *roofline* based approach which is able to derive which particular metric can lead to overall improvements in algorithmic fidelity, as well as upper bounds on these metrics past which no additional end-user gains can be expected. For example, when comparing Sycamore (Google) and CNOT (IBM) entangling gates for a particular algorithmic workload, our analyses show that there are ranges of relative gate fidelities where one configuration can always outperform the other. Once a certain *threshold* fidelity has been attained, no improvements in one- or two-qubit gate fidelity on any architecture can lead to better relative performance with respect to the other.

Next, we introduce a circuit synthesis based compilation procedure which indicates that the existing gate set design criteria that favors choosing gates based on their attainable fidelity and representational power of random two-qubit process may be misleading. Instead, our analysis shows that the criteria

should be augmented with their representational power for multi-qubit processes (e.g. three qubit) that are drawn from implementations of existing algorithms. For example, while the B-gate [50] is the most expressive gate for two qubit unitaries, we cannot uncover advantages when using it to represent complex programs. When compared against CNOT, B-gates lead to gate count increases and possible fidelity decreases. At the other end of the spectrum, we show that several low-entanglement gates such as  $\sqrt[4]{\text{CNOT}}$  and  $\sqrt{i\text{SWAP}}$  are sometime able to offer similar expressive performance as maximally entangling gates for important circuits such as TFIM, QFT, and QAE, leading to better algorithmic fidelity.

As discussed in Section 11, we believe our assessment procedure extends well beyond NISQ into the Fault Tolerant era of quantum computing.

## 2 Background

### 2.1 Quantum Computing Basics

The fundamental unit of information in a quantum computer is the qubit, which can be represented as a vector of the form

$$|\psi\rangle = \alpha \begin{bmatrix} 1 \\ 0 \end{bmatrix} + \beta \begin{bmatrix} 0 \\ 1 \end{bmatrix}$$

where  $\alpha$  and  $\beta$  are complex numbers such that  $|\alpha|^2 + |\beta|^2 = 1$  and  $\begin{bmatrix} 1 \\ 0 \end{bmatrix}$  and  $\begin{bmatrix} 0 \\ 1 \end{bmatrix}$  are orthonormal basis vectors representing the two distinct quantum states.

These basis vectors can also be written in Dirac notation as  $|0\rangle = \begin{bmatrix} 1 \\ 0 \end{bmatrix}$  and  $|1\rangle = \begin{bmatrix} 0 \\ 1 \end{bmatrix}$ .  $|\alpha|^2$  and  $|\beta|^2$  represent the probability of measuring  $|0\rangle$  and  $|1\rangle$  respectively. As  $\alpha$  and  $\beta$  are complex numbers, this qubit has both an amplitude associated with each basis state, as well as a additional relative phase between the two numbers which cannot be measured directly <sup>1</sup>, but can be leveraged for speedup in quantum algorithms.

The state of a quantum system with  $n$  qubits in states  $|\psi_1\rangle, |\psi_2\rangle, \dots |\psi_n\rangle$  lies in a  $2^n \times 2^n$  Hilbert space, and can be represented by the tensor product  $|\psi_1\rangle \otimes |\psi_2\rangle \otimes \dots \otimes |\psi_n\rangle$ . This quantum state  $|\psi\rangle$  can be evolved by use of  $2^n \times 2^n$  unitary operators[34]. Any  $n$ -qubit unitary can be broken down into a set of smaller unitaries, typically 1 or 2 qubit unitary gates. This series of gates can be drawn using the quantum circuit model [14]. Single qubit and multi-qubit gates act on qubits which are drawn as horizontal wires (see Figure 1). The number of wires or qubits  $n$  is called the circuit width, while the length or depth of the circuit is  $T$ . The depth is typically drawn as the x-axis of the circuit.

<sup>1</sup>The phase cannot be measured directly in the standard Z-basis corresponding to the basis states  $|0\rangle$  and  $|1\rangle$ , but can be measured in other bases

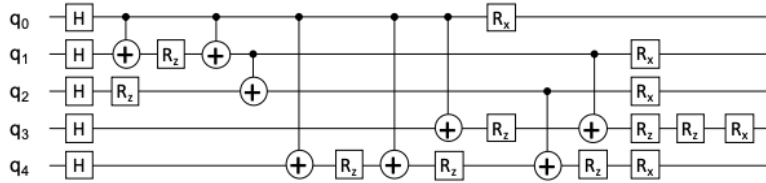


**Figure 1:** Example quantum circuit with 5 qubits broken down into the native gates of the device. Each qubit is represented by a horizontal line, and the timing of the circuit is described by the x-axis. In this case, the native gates consist of the  $H$ ,  $R_z$ ,  $R_x$  1-qubit gates and the 2-qubit  $CNOT$  gate.

## 2.2 Quantum Devices

Today’s quantum computers span a range of underlying qubit technologies. Each technology designates its own restrictions. Today, the most popular technologies being researched are Superconducting, Ion Trap, and Neutral Atom computers. Superconducting qubits are built into 2D silicon chips, which allows them to scale quickly, but means they are fixed in place. As quantum gates are difficult to apply over large distances, superconducting qubits can typically only interact with their nearest neighbors (local links). This restriction enforces a *physical topology* on the device, which is typically a grid or other 2D planar graph. When breaking down a large unitary, compilers must ensure that only these local interactions are used. This process of compiling a large unitary to a physical topology is called *mapping and routing*. Ion Trap and Neutral Atom computers operate on atoms, which can be moved around to interact with any other qubit. This gives them an all-to-all connectivity, albeit at the cost of moving around their qubits.

## 2.3 Quantum Gates

A quantum gate can be considered an elementary operation of a given quantum computer, similar to logic gates on a classical computer. The set of gates that a device offers that a larger unitary can be broken down into is called the *native gate set*. This gate set is universal if it can represent any  $n$ -qubit unitary with arbitrary precision. The list of these native gate sets are shown in Table 1. The compiler is responsible for translating the initial quantum circuit to only use gates that are available in a device’s native gate set.

The gates available on a given machine are a function of the underlying physics as well as the algorithmic workload that will be targeted. As previously mentioned, current 2-qubit gate design finds a gate that is “good enough” to represent arbitrary unitaries and can be implemented with high fidelity. In this case, “good enough” typically signifies a gate in the  $CNOT$  Family (gates that are equivalent to  $CNOT$ s up to single-qubit rotations, which are relatively cheap to apply). These gates include  $CNOT$ ,  $ECR$ ,  $ZZ$ ,  $XX$ , and  $CZ$  gates.  $CNOT$ s are

the most common gate in quantum algorithms as they are easy to understand (quantum equivalent to an XOR gate). This makes this set of gates a good idea to target with hardware, even at the potential cost of implementation, since they are simple to convert to from most CNOT-based algorithms. Other gates that are offered may be implemented more efficiently for a given device while potentially suffering from poor re-targeting of a variety algorithms. This trade off is explored throughout this paper.

Quantum gates are either *constant* or *parameterized*. A constant gate implements a single fixed unitary (e.g CNOT, X, Z). A parameterized gate takes in a set of continuous parameters, which typically correlate to angles of rotation along different axes. For example the single-qubit U3 gate takes in 3 parameters which correspond to angles for an X, Y, and Z rotation. As parameterized gates are continuous, the set of parameters can be differentiated over and optimized [48]. While parameterized gates are far more flexible and powerful, they are much harder to calibrate and this can result in lower fidelities. As 2-qubit gates are more difficult to implement, they are typically implemented as constant gates (although the XY gate and FSim gate provide 2 exceptions which we explore later in section 8.4).

Current quantum machines typically offer parameterized single-qubit gates. These single-qubit gates can be composed to perform any single-qubit unitary operator. 2-qubit gates are responsible for performing *quantum entanglement* between 2-qubits. All of the vendor-provided quantum gates are entangling, and we explore the strength of these entanglements more in Section 11. A quantum computer that is able to perform any single-qubit operation and entangle qubits is universal.

## 2.4 Sources of Qubit Error

Errors in quantum bits are caused by unwanted interactions with the environment. As these quantum systems are extremely hard to isolate, errors are prevalent in today’s NISQ computers. Because of this, the most important metric to optimize for in NISQ systems is qubit fidelity, which defines how close a qubit state is to the ideal state. Qubit fidelity is defined as a number between 0 and 1, where 0 represents a qubit state that is orthogonal to the correct state, and 1 indicates that the states are identical.

### 2.4.1 Qubit Decoherence

Qubits are only able to keep their quantum state for a period of time. This is known as the coherence time. The T1 coherence time is a measure of how long a qubit can maintain the correct amplitudes of  $\alpha$  and  $\beta$  before decohering to the low-level  $|0\rangle$  state. The T2 time corresponds to how long the state maintains its relative phase.

Today, these times sit at around 130 microseconds for T1 times and 100 microseconds for T2 times [21]. They vary greatly between different quantum technologies and even between qubits in the same computer.



### 2.4.2 Gate Error

In addition to decoherence, applying operations to qubits is also very costly. Each gate may introduce additional noise, which can be modeled as the qubit being acted on by an erroneous channel with a probability of error  $p$ <sup>2</sup>. As shown in Table 1, single-qubit error rate is reasonably low (on the order of  $10^{-3}$ ). On the other hand, two-qubit gates are much higher ( $10^{-2}$ ) and have much higher variance amongst the different links in a machine. These two-qubit gates are essential to quantum algorithms, as they allow for qubits to entangle, which provides the speedup for most use cases. Therefore, minimizing the number of gates, and especially the number of two-qubit gates, is very important for an effective compiler, as the gate count is negatively correlated with the fidelity of the final qubit state.

### 2.4.3 Measurement/Readout Error

Similar to gate errors, measuring a quantum state may also introduce noise. These errors are also on the order of  $10^{-2}$  [21] but are outside the scope of this paper.

### 2.4.4 Cross Talk Error

The errors we have considered thus far have all been assumed to be localized and independent. This is an important assumption, especially in the field of Quantum Error Correction [34]. However, entangled qubits that are acted upon may cause correlated errors (cross talk) between nearby qubits. Cross talk errors can be caused by several factors, including but not limited to: unaccounted entanglement of qubits, electromagnetic radiation when manipulating another qubit, entanglement that occurs on readout, etc. There have been attempts to properly model cross talk noise under the Markov assumption for these errors [42] and we introduce fidelity models in Section 8 that aim to capture this noise.

## 3 Quantum Hardware Characterization and Benchmarking

Today’s systems are dominated by superconducting (IBM, Google) and trapped ion (Quantinuum, IonQ) qubits. Neutral Atom (QuEra, Atom Computing) and silicon-spin qubits (Intel) are starting to gain traction, while several other technologies are continuously being developed. All these systems expose to end-users a universal gate set [34], composed of single-qubit and entangling two-qubit

---

<sup>2</sup>This is a simplification of the Kraus Operator formalism of an erroneous channel. There is an associated probability for all possible errors, but through randomized benchmarking, this can be captured by a single probability.

Hardware	Num Qubits	Technology	Connectivity	Native Gate Set	1Q/2Q Error (RB/XEB)
Google Sycamore	54	Superconducting	2D NN	1Q: XZ, RZ 2Q: FSim, $\sqrt{i}$ SWAP, Sycamore, CZ	0.001 / 0.01
IBM Eagle r3	127	Superconducting	2D NN	1Q: SX, RZ, X 2Q: ECR	0.0002 / 0.007
IBM Hummingbird r3	65	Superconducting	2D NN	1Q: RZ, SX, X 2Q: CNOT	0.00027 / 0.012
IBM Falcon r5	27	Superconducting	2D NN	1Q: RZ, SX, X 2Q: CNOT	0.0003 / 0.0079
Rigetti Aspen M3	79	Superconducting	2D NN	1Q: RX, RZ 2q: CZ, XY	0.001 / 0.14, 0.092
Quantinuum H2	32	Ion Trap	A2A	1Q: U1, RZ 2Q: ZZ	3e-5 / 0.002
IonQ Forte (2024)	35	Ion Trap	A2A	1Q: GPi, 2Q: ZZ, XX	0.0002 / 0.0040
IonQ Aria	21	Ion Trap	A2A	1Q: GPi, 2Q: XX	0.0006 / 0.0040

**Table 1:** Summary of existing commercial Quantum Computing hardware [37, 15, 40, 22, 3]. As we can see, most devices available now are superconducting or ion trap devices, with superconducting devices proving to be easier to scale. This contrasts the ion trap devices which show on average higher RB fidelity. Additionally, superconducting qubits have a 2D NN (2D Nearest Neighbor/mesh) topology while ion traps are all-to-all (A2A).

native gates. These gate-set choices are outlined in Table 1. Several methods exist to characterize today’s quantum machines:

**Average Gate Fidelity:** The widest used characterization and processor optimization metric is the *average gate fidelity*, which captures the probability that a state does not succumb to any error when a gate is applied. Fidelity can be measured using Randomized Benchmarking (RB) protocols [31, 30, 25], which use random circuits to generate an error channel with a single probability  $p$ , the average infidelity of the channel. By varying the depth of the circuits, existing protocols calculate the infidelity per gate ( $p_{\text{gate}}$ ): fidelity is then computed as  $1 - p_{\text{gate}}$ .

In 2019, Google introduced the cross entropy benchmarking (XEB) protocol [2] as another way to compute average gate fidelity. Importantly, this study also shows that the total average fidelity of a circuit can be approximated using a simple *digital error model*, validated for NISQ size systems.

**Process Fidelity:** As RB protocols have trouble scaling past three qubit processes, Cycle Benchmarking (CB) [17] has been proposed to improve characterization scalability to larger processes (and hardware). CB based protocols indicate that besides average gate fidelity, hardware dependent metrics such as qubit connectivity and algorithm specific metrics such as gate parallelism per cycle need to be taken into account when assessing algorithm fidelity.

**Quantum Volume:** Quantum Volume (QV) [12] characterizes the capability of hardware to execute random circuits of a certain size. This metric cannot be used to compare the fidelity of different process implementations running on the same machine or that of a single process running across different machines.

**Algorithmic Qubits:** IonQ’s Algorithmic Qubits (AQ) metric [9] captures a system’s ability to execute an algorithmic workload. AQ protocols measure the largest number of effectively perfect qubits you can deploy for a typical quantum program. It is similar to QV, but it additionally considers quantum error correction and presents a clear and direct relationship to qubit count. The AQ metric captures the impact of the compilation tool-chain.

All of these protocols and metrics reveal different useful information about a single configuration of quantum machine. However, they all fail when comparing across different hardware and gate sets. While we can measure the fidelity and quantum volume of a CNOT-based machine and of a Sycamore-based machine, this does not give us any information on their respective abilities to run a given algorithm. AQ encapsulates the algorithmic potential of different hardware, but it is still unable to quantify the degree to which one needs make changes to an architecture’s configuration in order to provide better comparative performance.

In order to make these inferences, we advocate for an algorithmic workload based approach centered around circuit fidelity models that combine hardware characterization metrics with the hardware’s ability to represent and implement a particular algorithm. We start with the simple digital model based on average gate fidelity, which we then extend to account for crosstalk due to parallel gate execution as well as qubit connectivity (an idle qubit can be affected when executing an operation on a neighboring qubits).

### 3.1 Roofline

The *roofline* model [47] provides an intuitive understanding of performance bottlenecks in classical hardware. The model outputs the maximum attainable performance on a machine as a function of the operational intensity of an application. This allows hardware and software architects to understand the inherent limits of their design in the context of important universal metrics: computational power and network bandwidth.

Our paper introduces a quantum analog, which highlights bottlenecks in algorithmic fidelity when comparing two different machines by gate expressivity, fidelity, and connectivity. While the classical roofline is fixed for a particular hardware, our relative roofline is fixed for an algorithmic workload. This allows for simple comparisons to be made between quantum computers for targeted domains. As a consequence, our model is compiler dependent, which motivates our custom compiler workflow and the importance of numerical synthesis based transpilation (Section 4.2).

## 4 Quantum Algorithms and Compilers

As we have introduced, minimizing the number of gates in a circuit and the average error introduced by each gate will improve algorithmic fidelity. The gate count for a given algorithm implementation is determined by hardware characteristics: 1) representational power of the native gate set; and 2) qubit interconnection topology.

Due to exponentially compounding gate infidelities, the dominant factor in the total fidelity is gate count. This has two consequences: 1) comparisons between system configurations should be done using the implementation with the fewest number of gates attainable, together with the lowest depth or highest gate parallelism; and 2) the compilation tool-chain plays a very important role in determining the overall “performance” of a given configuration.

### 4.1 Quantum Algorithms

Domain generators [33, 37] that produce the circuit associated with a given algorithm tend to have the following common characteristics:

- They are developed to generate circuits in a restricted gate set. Most generators use directly the CNOT gate, while some hardware-vendor-provided generators target only vendor supported native gates.
- The generated circuits have a logical qubit connectivity that resembles the domain level structure. For example, optimal QFT circuits are generated assuming an all-to-all qubit connectivity. Circuits generated for fermionic [33] interactions map fermions to qubits using a logical topology that resembles the structure of the physical system modeled.

- Some generators are deemed optimal. Optimality here relates only to asymptotic complexity: a good compiler can greatly reduce the constants that appear in the complexity formula.

Due to these properties, a quantum compiler’s ability to: 1) eliminate gates that are redundant or can be simplified from the circuit; 2) map and route the input circuit to the hardware configuration; and 3) translate (transpile) the input circuit to a different gate set is paramount for accurate architectural comparisons.

## 4.2 Quantum Compilers

Traditional vendor compilers use peephole optimizations based on 2-qubit gate synthesis (KAK decomposition [45]), application of gate commutativity rules, or domain specific pattern rewriting rules (*e.g.* Tket’s phase gadgets [11]). They also provide mapping and routing algorithms [37, 44, 26] and translation between multiple gate sets (“transpilation”). In particular, transpilation is performed using a 1:1 gate rewriting rule: any 2-qubit gate is rewritten directly from one (*e.g.* CNOT) to another (*e.g.* Sycamore).

Benchmark	Size	Gate	BQSKit		Tket		Cirq		Qiskit	
			a2a	mesh	a2a	mesh	a2a	mesh	a2a	mesh
mul_10	163									
		cz	<b>67</b>	<b>89</b>	104	134	134	227	132	141
		b	<b>110</b>	<b>125</b>	208	480	-	-	-	-
		syc	<b>103</b>	<b>139</b>	208	319	260	364	-	-
qft_16	264	cz	<b>237</b>	<b>336</b>	240	522	264	563	264	426
		b	<b>242</b>	<b>302</b>	480	1044	-	-	-	-
		syc	<b>241</b>	<b>365</b>	480	828	288	755	-	-
TFIM_16	240	cz	<b>200</b>	<b>200</b>	240	240	240	240	240	240
		b	<b>200</b>	<b>202</b>	480	480	-	-	-	-
		syc	<b>200</b>	<b>208</b>	480	219	440	440	-	-

**Table 2:** Comparison of two qubit gate counts for a subset of the benchmarks and gate sets across our different compilers. The first number under each compiler is for an all-to-all topology system, while the second number is for a mesh topology. Synthesis based compilers, such as BQSKit, produce the circuits with the least amount of gates. Note that Cirq (Qiskit) is unable to compile to the B Gate (B and Sycamore Gate).

### 4.2.1 Circuit Synthesis

Numerical circuit synthesis [49, 39] based tools have been introduced recently and have been shown to provide better quality implementations [13, 29, 48, 46] when compared against vendor compilers, albeit at the expense of increased compilation time. Numerical synthesis uses iterative optimization to approximate a unitary with bounded error while trying to minimize the number of gates. Some of these tools integrate optimization [13] with mapping [29] and gate transpilation [48]. They can search a large space of circuit structures and transformations.

All compilation tools have one thing in common: the compilation workflow is custom and it consists of repeated applications of passes and transformations. While it is hard to quantify the impact of optimization, mapping, and transpilation phases in isolation, we note that compilers can realize up to an order of magnitude in gate count reduction, even when the input circuit is “optimally” generated.

Family	Benchmarks (circuit_width)
TFIM	TFIM_16, TFIM_64, TFX_Y_16, TFX_Y_64
QAE	qae_9, qae_13, qae_17, qae_21
QFT	qft_4, qft_12, qft_64
QAOA	qaoa_10
QPE	qpe_14, qpe_18
Adder	adder_9, adder_63, mul_10, mult_60
Shor	shor_12, shor_16, shor_24, shor_28
Grover	grover_5
Hubbard	hubbard_4, hubbard_8, hubbard_12
QML	qml_6, qml_13, qml_22
VQA	vqe_12 (LiH), vqe_14 (BeH <sub>2</sub> )

**Table 3:** Our Benchmarks: List of benchmark circuits organized by family. Each circuit was initially created with CNOT and U3 gates.

## 5 Evaluation Procedure

We used the algorithms shown in Table 3 for our evaluation. They include many important categories including Variational Algorithms (VQA and QAOA) [36, 18], Finance (QAE) [19], Number Theory (QFT, QPE, Shor) [6], Physical Simulation (Hubbard, Ising(TFIM)) [7, 43], Search (Grover [32]), and Quantum Machine Learning (QML). The QML circuit is based on [8] and has an n-bit encoder and a two-local network. Most benchmarks were generated using Qiskit circuit generators[37], while the TFIM circuits were generated with F3C++ compiler [35]. For each algorithm we generate several instances across inputs and circuit sizes (number of qubits). Overall, we believe that our algorithmic workload provides a good sampling of the space of circuit implementations. We consider up to 64 qubit programs, with gate counts as high as 37000 accounting for a maximum depth of 44500. The logical topology of these programs ranges from linear in TFIM to all-to-all in QFT.

We translate and optimize the benchmarks for native gates present in today’s hardware (CNOT, ECR, CZ, ZZ, XX, Sycamore,  $\sqrt{i}$ SWAP), as shown in Table 1. Additionally, we examine experimental gates theorized to provide algorithmic fidelity advantages due to either high expressivity or high fidelity, B and  $\sqrt[4]{\text{CNOT}}$  or  $\sqrt[8]{\text{CNOT}}$  respectively.

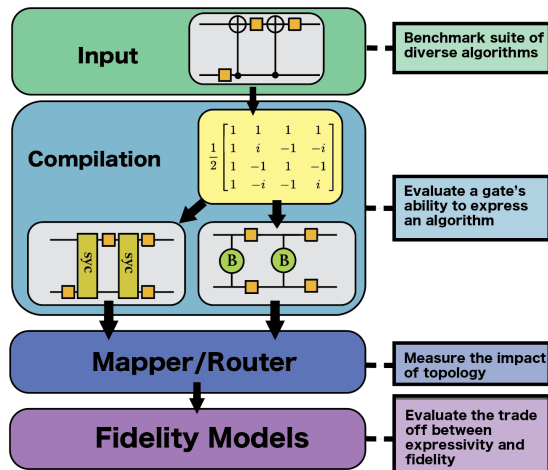


**Figure 2:** Our Hardware Comparison Procedure: A synthesis-based cross-compilation process (sometimes called “transpilation”) allows us to explore multiple gate sets and the ability to express an algorithm in terms of gate count, depth, and parallelism. From there, we can understand the effects of topology and fidelity on the overall performance of a quantum machine.

An overview of our process is shown in Figure 2. We use a custom compilation workflow that composes compilers (Qiskit, Cirq, Tket) with the BQSKit [49] circuit synthesis tools and selects the best resultant circuits. This workflow combines rule-based and algorithm-level transformations (Tket, Qiskit) with the power of multi-qubit translation offered by numerical synthesis. When translating between gate sets, numerical synthesis performs global optimizations of multi-qubit circuits, which leads to better results compared to peephole pattern replacement and 1:1 gate translation offered by vendor compilers. Table 2 shows a sampling of these results. While details of the compilation workflow are beyond the scope of this paper, to our knowledge, we generate the best attainable implementations of a given algorithm on a given hardware configuration. These resource “optimal” circuits<sup>3</sup> are then run through our fidelity models described in Section 7 in order to compare overall performance.

## 6 Gate Representational Power

Given a reference implementation using CNOT gates, in Figure 3 we show the relative two-qubit gate count (averaged across circuit families) after re-targeting to a particular gate. This data shows the ability of a gate to represent a particular algorithm, i.e. it captures its expressivity and entanglement power. When considering existing native gates, the {CZ, ZZ, XX, ECR} set seems to have the same representational power as CNOT gates. The native gates {Sycamore,

<sup>3</sup>Meaning they do not improve with further compilation and optimization.

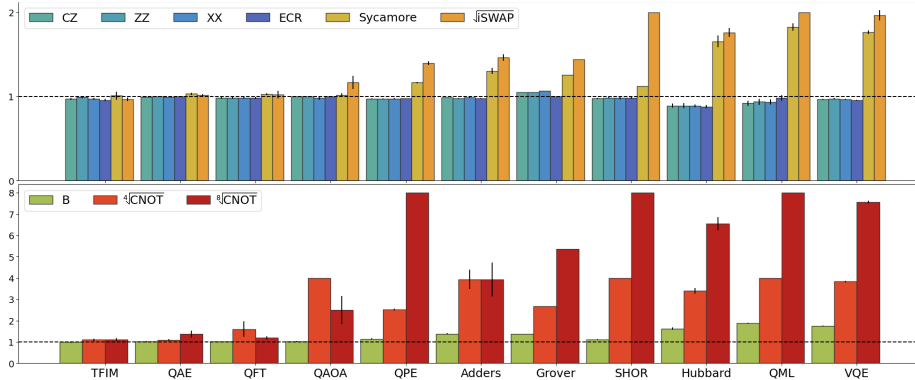


**Figure 3:** Normalized two-qubit gate count for existing hardware (top) and theorized hardware (bottom). We plot the relative count with respect to the optimally compiled CNOT based circuit. The gate count encapsulates logical algorithm connectivity and serves as a proxy for a gate’s ability to represent the algorithm.

$\sqrt{i}$ SWAP} have lower representational power than CNOT, as illustrated by their higher gate counts. When considering theorized gates, we see that  $\{B, \sqrt[4]{\text{CNOT}}, \sqrt[8]{\text{CNOT}}\}$  have overall lower representational power than CNOT. This is surprising as the motivation behind the introduction of the B-gate was its optimal 2-qubit representational power.

This behavior is also algorithm dependent. The TFIM, QAE, and QFT circuits require almost the same number of gates, irrespective of which gate it is used. For the rest of the circuits, we see more nuanced behavior. The gate set  $\{\text{CZ}, \text{ZZ}, \text{XX}, \text{ECR}, \text{CNOT}\}$  leads to the least amount of gates used, with much higher gate counts for the set  $\{\text{Sycamore}, \sqrt{i}\text{SWAP}, B, \sqrt[4]{\text{CNOT}}, \sqrt[8]{\text{CNOT}}\}$ .

This data indicates that the machine with the highest gate fidelity will be best suited to execute TFIM, QFT, and QAE. For the rest of the algorithms, the best machine will consider trade offs in both gate fidelity and circuit structure (gate count, parallelism etc.). Our data also indicates that gate representational power with respect to full algorithms needs to be taken into account when selecting a system configuration. We discuss in detail representational power trade-offs in Section 10.

## 7 Circuit Fidelity Models

In the NISQ era, it is critical to maximize the probability that a circuit’s output state is correct. The output expectation can be described a function of the average gate fidelity of the machine, written as [34]:

$$\mathbf{F}_{\text{gate}}(\mathcal{E}, U) = \int d\psi \langle \psi | U^\dagger \mathcal{E}(\psi) U | \psi \rangle$$

where  $U$  is the target unitary and  $\mathcal{E}$  is the erroneous channel trying to implement  $U$ .



To assess algorithm fidelity on a particular system configuration, we use a series of models that capture circuit characteristics together with an increasing number of architectural features: (1) gate fidelity; (2) gate fidelity and parallelism. In Section 8.5 we discuss a model based on qubit connectivity as well.

Let  $\mathbf{F}(\cdot)$  denote a circuit fidelity model, and let  $A$  and  $B$  denote two distinct system configurations. In order to enable system comparisons, we analyze the *objective function* given by:

$$\pi = \mathbf{F}^A(\cdot) - \mathbf{F}^B(\cdot)$$

## 7.1 Gate Fidelity

Our first model is derived from [2], in which the authors verify that the measured fidelity and estimated fidelity based on this model track almost exactly for their tested circuits.

**Definition 7.1 (Digital Fidelity Model).** The average circuit fidelity  $\mathbf{F}_d$  can be estimated as

$$\mathbf{F}_d = \prod_{i=1,2,..} f_i^{n_i}$$

where  $n_i$  is the number of  $i$ -qubit gates in the circuit, and  $f_i$  is the average fidelity of an  $i$ -qubit gate. For systems with only one- and two-qubit native gates this becomes:

$$\mathbf{F}_d = f_1^{n_1} \cdot f_2^{n_2}$$

with the objective function:

$$\pi_d = f_1^{A n_1^A} \cdot f_2^{A n_2^A} - f_1^{B n_1^B} \cdot f_2^{B n_2^B}$$

## 7.2 Gate Fidelity and Parallelism

In many systems, parallel execution impacts the attainable gate average fidelity. To capture this, we use a model based on Cyclic Benchmarking [17]. The protocol considers circuits as a series of cycles, with which we can calculate a single cycle fidelity as function of the 1-qubit and 2-qubit process fidelities ( $\gamma$ ). The process fidelity and average fidelity as defined above are related by a simple linear equation [20].

**Definition 7.2 (Cyclic Fidelity Model).**

$$\mathbf{F}_c = \prod (1 - e_i \cdot P_i)^m$$

where  $P_i$  is the average parallelism of  $i$ -qubit gates in the circuit, and  $e_i$  is the average process infidelity for an  $i$  qubit gate ( $1 - \gamma_i$ ).  $e_i$  can be measured using the Cycle Benchmarking protocol. The objective function for our machine comparison becomes:

$$\begin{aligned}
\pi_{\mathbf{c}} &= \mathbf{F}_{\mathbf{c}}^A - \mathbf{F}_{\mathbf{c}}^B \\
&= (1 - e_1^A \cdot P_1^A)^{m^A} \cdot (1 - e_2^A \cdot P_2^A)^{m^A} \\
&\quad - (1 - e_1^B \cdot P_1^B)^{m^B} \cdot (1 - e_2^B \cdot P_2^B)^{m^B}
\end{aligned}$$

## 8 Evaluating Quantum Machines

Now, we can finally answer the question “*What machine should I use to run my algorithm?*”.

The answer is rendered trivial when considering currently published gate fidelity figures. Quantinuum boasts by far the highest 2-qubit gate fidelity at 0.998 and its ZZ gate can express our algorithmic workload well. For algorithms that use more qubits than H2’s capacity, the models suggest the IBM Eagle system.

A more insightful question is how could system configurations be changed in order to improve competitiveness, e.g. : “*How can other machines become better than H2?*”.

### 8.1 Quantifying Design Trade-offs

Our procedure allows us to quantify the trade-offs between a gate’s representational power for an algorithm and its fidelity. This is a comparative analysis where we vary the models’ parameters and solve for the objective function as defined in Section 7. As gates continue to improve and calibration/noise-mitigation techniques advance, architects and end-users must consider:

1. “What gate fidelity do I need in order to out-perform other machines? How does this vary by algorithm class?”
2. “Does single-qubit gate count matter for relative performance?”
3. “Is offering multiple entangling gates worth the development and maintenance effort?”
4. “How does the underlying chip topology affect the relative performance?”

Given that the maximum attainable gate fidelity is 1, in order to compare NISQ-era devices, we want to use realistic constraints. First, to simplify the model, we will initially limit the single-qubit gate type to only the  $U3$  gate. Current machines have parameterizable rotation gates that can be composed to perform any arbitrary single-qubit unitary. As 2-qubit gate errors still dominate, this simplification is justified. Based on Table 1, single-qubit gate fidelities vary from around 0.999 to 0.99999 across all quantum machines considered, while 2-qubit gates range from 0.990 to 0.999.

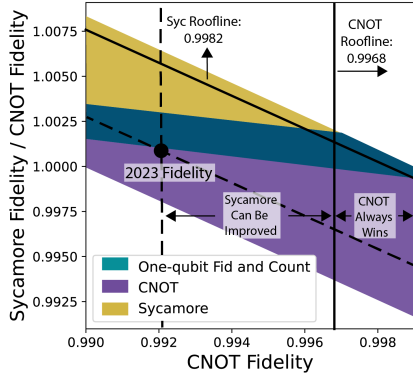


**Figure 4:** Machine capability to execute the *adder\_9* algorithm. CNOT fidelity is on the x-axis and the relative Sycamore fidelity on the y-axis. We plot the winning machine at each point. The middle area shows where the choice of best machine is a function of the single-qubit fidelity. In the other areas, each machine wins irrespective of 1-qubit gate fidelity. The published 2-qubit gate fidelities are shown with the black dotted lines, while the corresponding rooflines are plotted with solid black lines. The CNOT (Sycamore) gate always wins when its fidelity is right of (above) the roofline.

## 8.2 Two-Qubit Gate Analysis

We use the *adder\_9* algorithm to directly compare IBM Falcon (CNOT) with Google Sycamore (Sycamore) machines as our driving example. The corresponding objective function (defined in Section 7) is:

$$\pi_{\mathbf{d}} = f_1^{A70} \cdot f_2^{A49} - f_1^{B91} \cdot f_2^{B66}$$

For comparisons, we rewrite the objective function to use the Sycamore fidelity relative to CNOT. We vary the CNOT fidelity along the x-axis and the relative Sycamore fidelity along the y-axis. We then have two remaining free variables:

$$\pi_{\mathbf{d}} = f_1^{A70} \cdot x^{49} - f_1^{B91} \cdot (x \cdot y)^{66}$$

The results are summarized in Figure 4. Each point represents a two-system configuration we are comparing, with the 2-qubit fidelities set according to the  $x$  and  $y$  position. We identify three behavioral regions. In two regions, one configuration wins against the other, *no matter the single-qubit gate fidelity of*

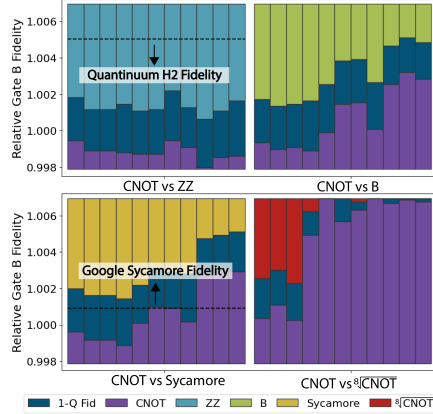


**Figure 5:** Gate set comparison against CNOT. CNOT fidelity is fixed to the IBM Falcon (vertical dotted line in Figure 4). The bars correspond to a vertical slice of the full analysis (Figure 4) for each of the circuit families: TFIM, QAE, QFT, QAOA, QPE, Adders, Grover, Shor, Hubbard, QML, and VQE. Encouragingly, low entanglement gates ( $\sqrt{\text{CNOT}}$ ) can provide better overall circuit fidelity for several important algorithms.

*the system.* In these regions 2-qubit gate fidelity and expressivity determine system behavior. In the central region, the behavior depends on the fidelity of single-qubit gates: one machine can be improved relative to the other by tuning their single-qubit gate fidelity. For each system we also compute a *2-qubit gate threshold fidelity*, shown with continuous lines: once that is reached on a system, no improvements<sup>4</sup> in the other system’s 2-qubit gate fidelity will change the overall ordering. We also plot the published fidelities of the respective hardware gates with a dotted line. The distance between actual and threshold fidelity for a gate indicates a window of opportunity to improve the other system.

We refer to this method of relative comparison as a *quantum hardware roofline*, as it allows us to compute bounds on the required improvements for a particular system configuration. For example, In Figure 4, once the CNOT gate reaches the *threshold* fidelity of 0.9968, no improvements in the Sycamore fidelity will outperform a CNOT based machine.

Figures 5 and 6 extend these results across algorithm classes and gatesets. Figure 5 compares several gates against the CNOT gate whose fidelity is fixed to that of the IBM Falcon system (each bar is a vertical slice of the plot in Figure 4 at the IBM Falcon fidelity). Again, configurations can be improved by improving only 2-qubit fidelity, or by improving 1-qubit and 2-qubit gate fidelity together. The exact behavior is algorithm and gate set dependent. Encouragingly, low entanglement gates can provide advantages for some algorithms. Figure 6 shows this behavior when targeting the Cyclic Model. The trends are similar across models, with the Cyclic Model placing a much smaller emphasis on the single-qubit configuration. This is to be expected since the model penalizes the impact of 2-qubit gates.

### 8.3 Single-Qubit Gate Analysis

To understand the implications for 1-qubit gate design we consider the closure of the 1-qubit dependent behavior (middle region) across “any” algorithm. To this end, we constrain the 1-qubit gate count as a function of the two-qubit gate count. We lower bound the 1-qubit gate count as  $\frac{1}{8}$  of the corresponding 2-qubit gate count, far below the ratio found in any of our experimental data. We upper bound with twice the 2-qubit gate count: any consecutive U3 gates can be combined into one, so there are at most two 1-qubit gates in between the 2-qubit gates.

Now, we can vary the 1-qubit gate count between these bounds (keep  $n_1^A$  and  $n_1^B$  as variables). Then, we can analyze how the objective function behavior changes as we fix single-qubit fidelity ( $F_1$ ) for both machines.

$$\pi = (F_1)^{n_1^A} \cdot x^{4153} - (F_1)^{n_1^B} \cdot y^{5944}$$

This analysis for *adder\_9* on the Falcon and Sycamore machines is shown in Figure 7. The 1-qubit dependent region shrinks as the 1-qubit fidelity improves, even as we allow for any single-qubit gate count. At some 1-qubit fidelity, the

---

<sup>4</sup>We vary the fidelities within the constraints of our model.

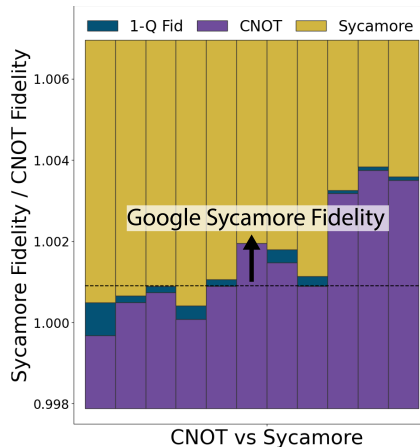


**Figure 6:** Sycamore Fidelity Comparison across algorithm classes using the cyclic fidelity model [17]. We see similar trends in terms of machine-dominant regions and rooflines, however the single-qubit impact is much smaller with this model.

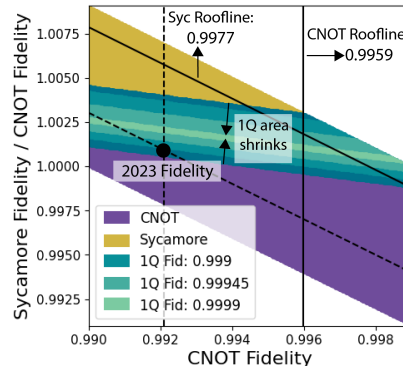


**Figure 7:** This plot shows the behavior of the 1-qubit dependent region as we fix the 1-qubit fidelity. The 1-qubit region shrinks as the fidelity increases, and disappears entirely when you reach a 1-qubit fidelity of 0.99998 for `adder_9`.

region completely disappears. We denote this as the *1-qubit threshold fidelity*: once this is reached, no improvement in 1-qubit gate fidelity will improve the relative performance between two machines.

We can solve for the threshold fidelity for different initial 2-qubit gate counts, as present in algorithms. We set up the objective function such that the 2-qubit counts for each machine are related by a ratio, and we vary this ratio along the x-axis in Figure 8.

$$\pi = y^{n_1^A} \cdot f_2^{A n_2^A} - y^{n_1^B} \cdot f_2^{B n_2^A \cdot x}$$

As shown in Figure 8, there is an upper bound ratio (3.5) where the threshold fidelity drops below the current worst NISQ-era worst single-qubit fidelities! For any two circuits where the 2-qubit gate ratio is higher than the upper bound (3.5), no improvements in the 1-qubit gate count on any machine can change relative performance. This explains why for several circuit families, the CNOT machine always beats the  $\sqrt[8]{\text{CNOT}}$  machine regardless of the single-qubit configuration!

We can then derive hardware-specific upper bound ratios which give direct information about the potential of changing relative performance in practice. Instead of using our generic bounds for our fidelity model, we use the 2-qubit gate fidelity ranges of existing machines and show results in Table 4. As indicated, the actual upper bounds are around 1.6, much lower than the 3.5 absolute threshold. Overall, this data indicates that for most systems, relative

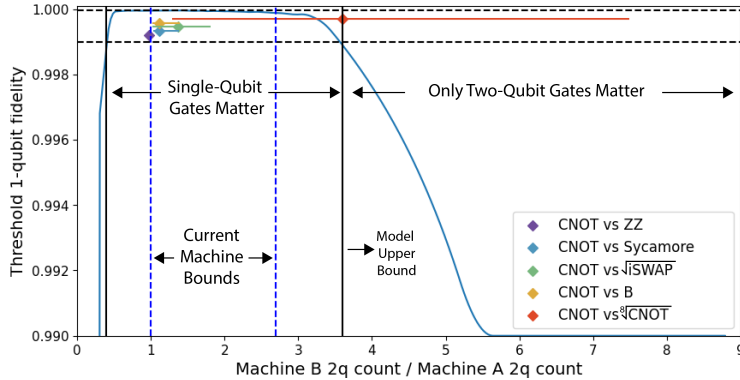


**Figure 8:** The X-axis shows the 2-qubit gate count ratio when comparing the implementations on two machines, while the Y-axis shows the resulting threshold 1-qubit fidelity. We also plot the range of 2-qubit gate count ratios we see for each gate compared to CNOT. The black dotted lines show the current NISQ single-qubit fidelity range. When using the upper bound on gate count ratio, the ordering of most machine comparisons is affected by the single-qubit gates. This quickly changes when we consider specific machines as shown in Table 4.

performance orderings can be changed by tuning 1-qubit gates. However, when comparing QML or Shor circuits on Falcon and Sycamore machines, algorithm and compiler designers should not focus on 1-qubit gate reduction in order to improve relative performance.

## 8.4 Mixing Entangling Gates

Systems such as Aspen and Sycamore offer multiple entangling gates and parameterized entangling gates. These gates will have different average fidelities and may be used together within a single circuit. In Figure 9 we show the 2-qubit gate counts for the Sycamore and Aspen machines when using parameterized and multiple 2-qubit entangling gates within the same circuit. Heterogeneous gate sets like Sycamore+ $\sqrt{i}$ SWAP and CZ+XY express circuits as well as the Sycamore or CZ gate alone, respectively. Therefore, on these systems choosing the highest fidelity gate for any algorithm may be sufficient.

The parameterized FSim gate leads to significant gate count reduction when compared to the Sycamore and  $\sqrt{i}$ SWAP gates, while the XY Gate provides no benefit over the CZ gate. The FSim gate takes two parameters, while the XY gate only has one. This allows the FSim gate to express complex unitaries more efficiently. Accordingly, FSim implementations can outperform Sycamore gate implementations even with a larger (0.4%) drop in fidelity! The circuit quality of the FSim gate may also point to a finite *spanning gate set* of FSim family gates that are able to express circuits as well as the full parameterized gate. A finite set of constant gates may prove to be easier to calibrate than a fully parameterized gate, leading to a higher gate fidelity.

Machine 1	Machine 2	Threshold
IBM Falcon	IBM Eagle	1.46
IBM Falcon	Google Sycamore	1.70
IBM Falcon	Quantinuum H2	1.06
IBM Eagle	Google Sycamore	2.69
IBM Eagle	Quantinuum H2	1.69
Google Sycamore	Quantinuum H2	1

**Table 4:** The upper bound on 2-qubit gates ratio that determines the impact of 1-qubit gate tuning for selected pairs of NISQ machines. We use gate fidelity provided by the data-sheets for each machine [15, 37, 38]. Gate count ratios less than the threshold ratio signify circuits where tuning 1-qubit gates can improve the relative performance. For Sycamore vs. H2 (1), the only way to improve relative performance is by improving 2-qubit gate fidelity, while for the Falcon vs. H2 (1.06) there is a slight window of opportunity.

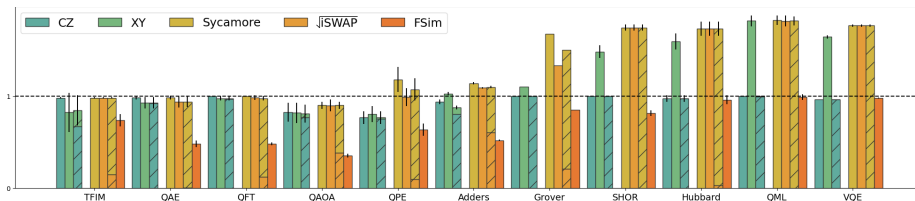


**Figure 9:** 2-qubit gate ratios relative to CNOT, for the Aspen and Google hardware systems. We show homogeneous implementations (CZ, Sycamore,  $\sqrt{i}$ SWAP), heterogeneous implementations (CZ+XY, Sycamore+ $\sqrt{i}$ SWAP), and parameterized entangling gates (XY, FSim). Heterogeneous implementations (stacked bars) are as good as homogeneous ones. The parameterized FSim gate is able to express every algorithm well and is worth targeting.

## 8.5 Topology

The physical qubit interconnection topology impacts system behavior by:

1. Increasing gate counts when the algorithm logical topology is mismatching, as shown in Figure 10.
2. Adding cross talk due to the device qubit couplings.

Architects can use our models to answer: “What fidelity improvement is needed to overcome a more restrictive topology?”. In Figure 11 we compare the capabilities of H2 (ZZ, all-to-all) with Sycamore (Sycamore, mesh) using the cyclic fidelity model. As before, we are able to identify ranges where a certain combination (gate, topology) performs best irrespective of 1-qubit gate fidelity, as well as ranges where relative performance depends on 1-qubit gate fidelity as well. The orange region in the graph shows the fidelity range in which Sycamore loses on account of being mapped to a more restrictive topology. The size of this orange region corresponds to the change in ability to express a circuit, and varies by algorithm.

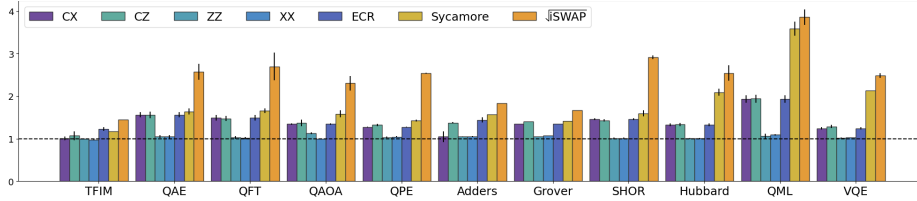


**Figure 10:** 2-qubit gate counts averaged across circuit families mapped to each device topology and gate set.

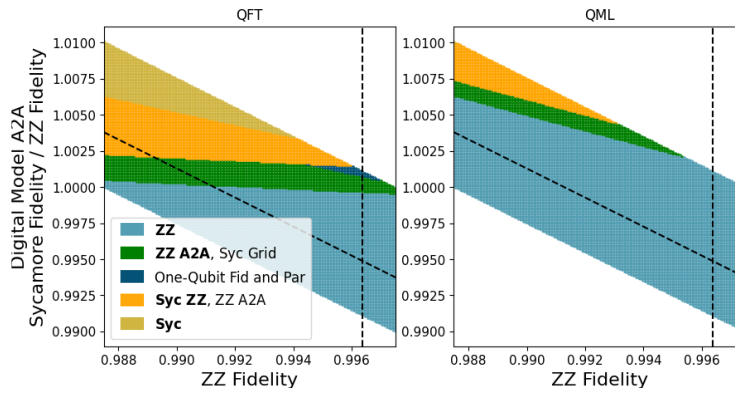


**Figure 11:** Topology effects for (ZZ, Sycamore) X (all-to-all, mesh). Dark blue region: relative performance can be changed by tuning 1-qubit fidelity. Light Blue region: ZZ always performs best, regardless of topology. Gold region: Sycamore always performs best. In the other regions, the bolded configuration performs best.



While Figure 11 is able to model the first effect of topology, we must turn to the coupling-based model introduced in [17] in order to understand cross talk:

$$\mathbf{F}_{\text{ctop}} = (1 - e_{c1} \cdot C_1)^{n_1} \cdot (1 - e_{c2} \cdot C_2)^{n_2}$$

where  $C_i$  is the number of other qubits on average that each qubit is coupled to and  $e_{ci}$  is the error per coupling for an  $i$ -qubit gate.  $C_i$  is a direct measure of the physical chip topology. For a grid topology, usually associated with superconducting qubits,  $C_2$  is a constant between 1 and 4. For all-to-all connectivities provided by ion traps  $C_2$  is instead  $\frac{1}{2}N(N-1)$ . The error per coupling is measured by the Cycle Benchmarking protocol, but these numbers are not provided for today’s devices.

## 9 Validation

These models trade off accuracy for tractability. While full noise simulation is able to give the most accurate view of algorithmic fidelity, it does not scale to system sizes of interest. However, we can use it as a point of comparison to validate the fidelity models we have chosen.

We first compare random circuits with varied gate count (see Figures 12a, 12b). We compare our digital model against two other models: full simulation and a depolarization channel model. We use Qiskit’s provided noisy backends which account for T1 and T2 coherence times of qubits, as well as explicit error channels for each gate application [37]. We expect the fidelity model to closely lower bound both other procedures, which we see in Figure 12a. Secondly, we ensure that our model outputs similar relative results as we vary the 2-qubit error for different gate sets. We show these experiments in Figure 12b for the *grover.5* circuit transpiled to a CNOT machine and a B-gate machine. We see that the relative performance remains the same as we vary the error.

We add further confirmation by running a full 2-qubit analysis as shown in Figure 4 using noisy simulation. As shown in Figure 12c, we see that the roofline numbers across both experiments closely match. We feel that the correlations seen in our model across these experiments in addition to the correlation seen in experiments run on real hardware [2, 17] validate the utility of our fidelity model.

## 10 Evaluating Gate Representational Power

A gate set’s ability to realize a circuit comes down to its expressivity and entanglement. Gate *expressivity* identifies a gate’s ability to represent a random two-qubit unitary. Architects often use the Weyl Chamber to directly visualize gate expressivity [28], as shown in Figure 13. The Weyl Chamber removes all non-local parameters from a 2-qubit unitary and plots it into a tetrahedron. Most 2-qubit gates can express any 2-qubit unitary in three applications (along with single qubit rotation gates). The most expressive gate, the B-gate, can

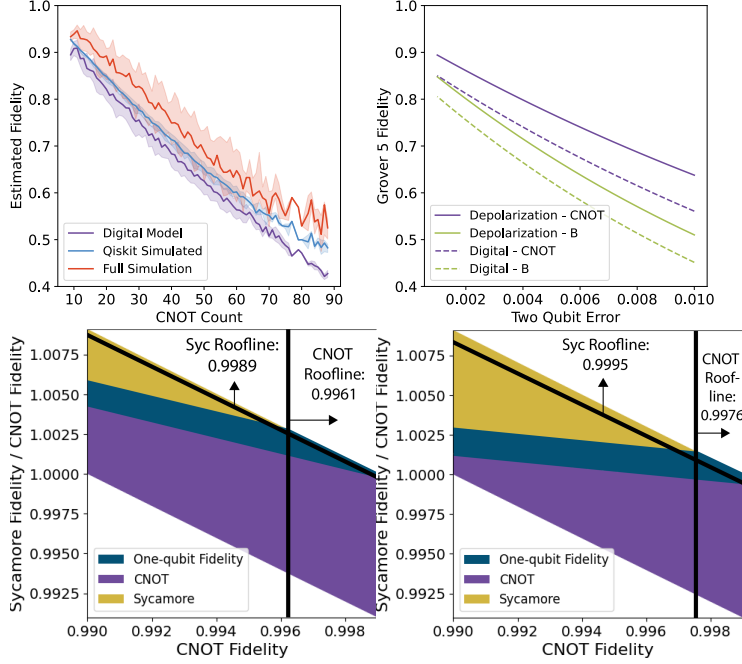


**Figure 12:** Validation experiments for our fidelity model. (a) Plot against full simulation on IBM Noisy Simulator and derived depolarization channel. We keep constant depth circuits with varied CNOT count gates. (b) Varying the 2-qubit gate error of our model vs. a general depolarization model. (c) and (d) 2-qubit gate analysis for adder\_9 and grover.5 respectively using fully noisy simulation. We see that the roofline numbers and regions closely match the behavior seen in Figure 4.

express any unitary in two applications (it can also easily be realized on a superconducting machine) [50].

Gate *entanglement* is a gate’s ability to maximize the entanglement between two qubits. CNOTs and most hardware native gates are maximally entangling, meaning that a single application to two qubits will leave them perfectly correlated. The  $\sqrt[4]{\text{CNOT}}$  and  $\sqrt[8]{\text{CNOT}}$  gates trade off entangling power for large potential gains in gate fidelity.

Several trends have become apparent in our research. Most notably, we see that with current state-of-the-art compilation, the B-gate does not lead to better circuits, nor does it increase fidelity. This is surprising, because the B-gate is the most expressive 2-qubit gate. On the other hand, we see some equally surprising positive results for the  $\sqrt[4]{\text{CNOT}}$  and  $\sqrt[8]{\text{CNOT}}$  gates. These low entangling gates require 4 and 8 applications respectively to represent a single CNOT gate. This makes their comparable expressivity in important circuits such as QFT, TFIM, and QAE circuits exciting.

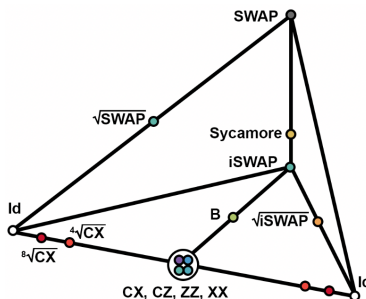


**Figure 13:** Projection of various 2-qubit gates onto the Weyl Chamber. Gates located at the same point represent unitaries that differ by single qubit rotations applied to each qubit (a 1:1 mapping).

## 10.1 Weyl Chamber Distribution of Two-Qubit Algorithm Blocks

Under our procedure, it is clear that the expressivity and entanglement of a native 2-qubit gate is not strongly correlated with algorithm performance under the currently accepted design criteria. While expressivity is assessed based on the power to implement random 2-qubit unitaries, optimal implementations of algorithms impose structure on the set of 2-qubit unitaries that these gates decompose.

To understand this structure, for any circuit represented in any gate set, we form maximal 2-qubit unitaries and plot their position within the Weyl chamber, as shown in Figure 14.

The distribution of 2-qubit unitaries drawn from circuits is not random. The input structure of the Adder group is spread out (it contains diverse unitaries), and it so happens that expressive gates, such as B, have trouble representing some of them. On the other hand, the input structure of the QFT algorithm is more periodic which allows Sycamore and B-gates to represent it well.

## 10.2 Synthesis Derived Gate Selection Criteria

The incorporation of circuit synthesis in our compilation workflow enables us to derive additional criteria for gate selection and development. The advantages derived from our flow are due to synthesis' powerful compilation capabilities.

Given an input circuit, traditional compilers will use local peepholes optimizations, translating from one gate set to another using analytical, one-to-one gate rewriting rules for 2-qubit gates. For example, a CNOT is translated into a sequence of two Sycamore gates and additional U3 gates. Any 2-qubit unitary can be represented using at most three CNOT gates. Thus it is expected to use more Sycamore than CNOT gates to represent an arbitrary 2-qubit gate. As mentioned, it takes at most two B-gates to implement random 2-qubit processes.

One-to-one gate rewriting has been shown to be less than optimal [48].

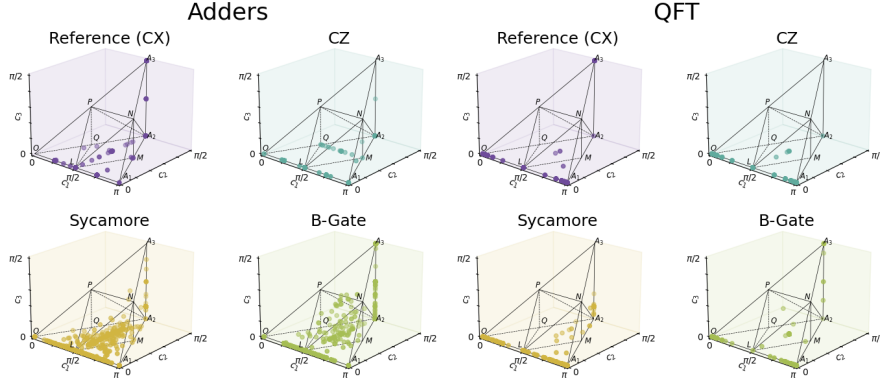


**Figure 14:** Position in the Weyl chamber of 2-qubit unitaries/blocks that arise in the Adder group (left) and QFT group (right) for different native gates. The initial spread of Adder unitaries proves to be a very difficult pattern for the Sycamore and B-gates to instantiate, hence the massive increase in gate count. On the other hand, the relatively simple pattern we see in the QFT unitaries (series of controlled rotations) are able to be expressed optimally by Sycamore and B-gates.

BQSKit’s synthesis based compiler [49] employs a different strategy. Given an input circuit, BQSKit partitions it into multi-qubit blocks (partitions). Each partition is optimized and translated using optimal topology aware direct unitary synthesis [13], combined with a powerful synthesis based mapping and routing algorithm [29]. Thus, deploying synthesis leads to different conclusions than when using vendor provided compilers, as we see in Figure 15.

More insights can be gained by examining gate representational power to implement 3-qubit blocks/processes that arise in algorithm implementations. We use the BQSKit partitioner to decompose a circuit in maximal 3-qubit gates and then use direct synthesis to generate circuits targeting each native gate set. This procedure results in implementations for each block that use an optimal number of 2-qubit gates, irrespective of gate choice. We plot the gate count distribution of blocks in Figure 16. The CNOT family of gates unsurprisingly have a one-to-one mapping, but the story changes for the Sycamore and B-gates. Using Sycamore gates increases gate count, which is to be expected. On the other hand, we see that the B-gate is able to better express some more complicated blocks (5-7 CNOT blocks reduce to 4 B-gates). However, the overall gate count reduction is held back by the B-gate’s inability to express simpler blocks efficiently. While a larger block granularity (4+ qubits) would not remove all simple blocks from these circuits, it remains to be seen whether the average increased complexity in each block would allow the B-gate to outperform other gates.

Overall, this analysis indicates that existing gate design criteria should be augmented. In addition to choosing a gate based on attainable fidelity and its representational power for *random* 2-qubit unitaries, the gate representational

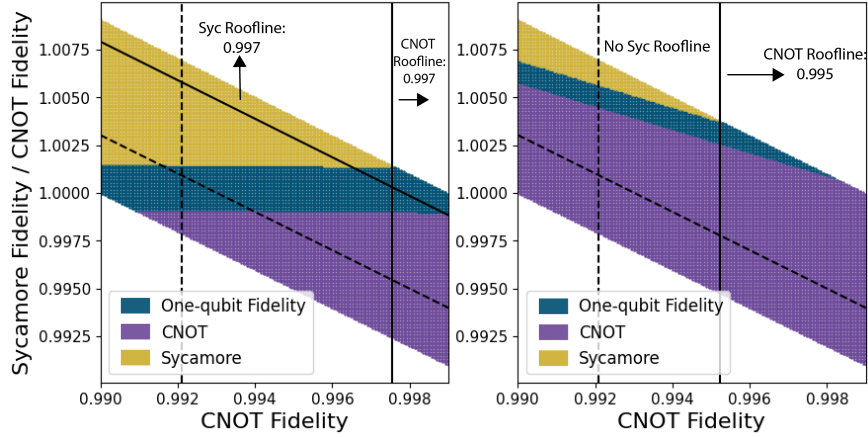


**Figure 15:** Comparison of fidelity plots when compiled with synthesis vs. Cirq. Non-local optimization leads to resource-efficient circuits for different gate sets, which results in vastly different comparisons. Note that under the Cirq compilation, there is no Sycamore roofline.

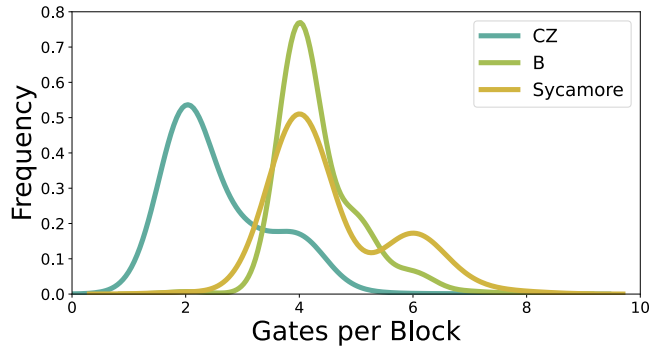


**Figure 16:** 2-qubit gate count distribution for the 3-qubit partitions present in the final compiled circuits of the Hubbard group. We compare the distribution of the CZ, Sycamore, and B Gate. The B-gate fails to express the simple blocks (fewer than 4 CNOT gates) efficiently but is able to simplify some of the longer blocks, while the Sycamore gate increases the number of gates across the board.

power for multi-qubit blocks (e.g. three qubit unitaries), drawn from implementations of real workloads, should be considered.

## 11 Discussion

While we have introduced and examined several models, we have emphasized the derivation of the roofline approach for the digital fidelity model. A similar derivation can be made for the cyclic model, emphasizing a relative roofline for 1-qubit and 2-qubit process fidelities. Each cycle’s fidelity has an absolute parallelism threshold of  $\frac{1}{P_i}$  according to the model, and this number will reduce as specific machines/circuits are targeted. We have also emphasized building a roofline model for hardware improvement by considering relative gate fidelity across two configurations. This derivation is useful to hardware designers and algorithm developers. By changing emphasis from fidelity to gate count and circuit depth, a similar derivation can produce roofline models for compiler developers to guide circuit optimization decisions: “What mix of gates to choose?; “Should I reduce gate count or increase gate parallelism?” etc.

Multiple studies [27, 41] have touched on the idea of co-designing quantum hardware, compilers and algorithms. This paper extends this process by considering device gate sets that target specific algorithms. For TFIM, QFT, and QAE circuits, we have shown that a designer should maximize gate fidelity even at the cost of expressivity and entanglement capability. On the other hand, we see highly expressive gates such as the B-gate provide little improvement in overall circuit fidelity.

We see that restricting the topology from an all-to-all connectivity leads to a potentially massive need for higher gate fidelity, varying by algorithm. This means that for Adder-based circuits, Hubbard models, or QML networks, an ion trap machine with a ZZ or XX gate is best suited.

Our results indicate that unlike classical benchmarking which is compiler independent, quantum system evaluation and benchmarking is sensitive to the quality of compilation tools. For the time being, the compilation workflow requires circuit synthesis for robust inferences.

We believe our methodology will apply beyond the NISQ era into the Fault Tolerant (FT) quantum regime. Every Quantum Error Correction Code (QEC) admits a *transversal gate set*. This is the set of gates that can be applied simply, without ever leaving the code space. However, as proved by Eastin and Knill [16], the set of gates in any transversal gate set is not universal. This requires a FT computer to admit a protocol for at least 1 non-transversal gate. There are several methods to apply a non-transversal gate, but they require large resource overhead in terms of additional qubits, latency, and cost. While for NISQ, we directly minimize two-qubit gate count, FT quantum computing requires minimization of this overhead. The choice of QEC, choice of non-transversal gate, as well as the choice of protocol to implement the non-transversal gate all suggest a new design space to which we can apply a similar analysis to the one in this paper.

## 12 Conclusion

In this paper, we introduce a procedure for performing comparisons between quantum system configurations. In our quantum roofline analysis, we derive bounds on system properties (e.g. gate fidelity) that can be used as a stop criteria for optimization efforts. We then evaluate machines across a large set of important algorithms and are able to quantify the trade-off required between gate fidelity, expressivity, and entanglement for different circuit families in order to maximize circuit execution fidelity. Our work also shows that the ability of circuit synthesis to generate resource minimal circuits is paramount to performance evaluation, and it enables new design criteria for gate set adoption. We believe our procedure is of interest not only to hardware designers, but compiler and algorithm developers as well.

## References

- [1] S. Aaronson and L. Chen, “Complexity-Theoretic Foundations of Quantum Supremacy Experiments,” *arXiv:1612.05903 [quant-ph]*, Dec. 2016, arXiv:1612.05903. [Online]. Available: <http://arxiv.org/abs/1612.05903>
- [2] F. Arute, K. Arya, R. Babbush, D. Bacon, J. C. Bardin, R. Barends, R. Biswas, S. Boixo, F. G. S. L. Brandao, D. A. Buell, B. Burkett, Y. Chen, Z. Chen, B. Chiaro, R. Collins, W. Courtney, A. Dunsworth, E. Farhi, B. Foxen, A. Fowler, C. Gidney, M. Giustina, R. Graff, K. Guerin, S. Habegger, M. P. Harrigan, M. J. Hartmann, A. Ho, M. R. Hoffmann, T. Huang, T. S. Humble, S. V. Isakov, E. Jeffrey, Z. Jiang, D. Kafri, K. Kechedzhi, J. Kelly, P. V. Klimov, S. Knysh, A. N. Korotkov, F. Kostritsa, D. Landhuis, M. Lindmark, E. Lucero, D. Lyakh, S. Mandra, J. R. McClean, M. McEwen, A. Megrant, X. Mi, K. Michielsen, M. Mohseni, J. Mutus, O. Naaman, M. Neeley, C. Neill, M. Y. Niu, E. Ostby, A. Petukhov, J. C. Platt, C. Quintana, E. G. Rieffel, P. Roushan, N. C. Rubin, D. Sank, K. J. Satzinger, V. Smelyanskiy, K. J. Sung, M. D. Trevithick, A. Vainsencher, B. Villalonga, T. White, Z. J. Yao, P. Yeh, A. Zalcman, H. Neven, and J. M. Martinis, “Supplementary information for ”Quantum supremacy using a programmable superconducting processor”,” *Nature*, vol. 574, no. 7779, pp. 505–510, Oct. 2019, arXiv:1910.11333 [quant-ph]. [Online]. Available: <http://arxiv.org/abs/1910.11333>
- [3] *Highly Scalable Quantum Computing With Atomic Arrays*, Atom Computing, 2023. [Online]. Available: <https://atom-computing.com/wp-content/uploads/2022/08/Atom-Computing-Atomic-Arrays.pdf>
- [4] F. Bao, H. Deng, D. Ding, R. Gao, X. Gao, C. Huang, X. Jiang, H.-S. Ku, Z. Li, X. Ma, X. Ni, J. Qin, Z. Song, H. Sun, C. Tang, T. Wang, F. Wu, T. Xia, W. Yu, F. Zhang, G. Zhang, X. Zhang, J. Zhou, X. Zhu,

- Y. Shi, J. Chen, H.-H. Zhao, and C. Deng, “Fluxonium: an alternative qubit platform for high-fidelity operations,” *Physical Review Letters*, vol. 129, no. 1, p. 010502, Jun. 2022, arXiv:2111.13504 [quant-ph]. [Online]. Available: <http://arxiv.org/abs/2111.13504>
- [5] R. Barends, J. Kelly, A. Megrant, D. Sank, E. Jeffrey, Y. Chen, Y. Yin, B. Chiaro, J. Mutus, C. Neill, P. O’Malley, P. Roushan, J. Wenner, T. C. White, A. N. Cleland, and J. M. Martinis, “Coherent josephson qubit suitable for scalable quantum integrated circuits,” *Phys. Rev. Lett.*, vol. 111, p. 080502, Aug 2013. [Online]. Available: <https://link.aps.org/doi/10.1103/PhysRevLett.111.080502>
- [6] S. Beauregard, “Circuit for Shor’s algorithm using  $2n+3$  qubits,” Feb. 2003, arXiv:quant-ph/0205095. [Online]. Available: <http://arxiv.org/abs/quant-ph/0205095>
- [7] S. Bravyi and A. Kitaev, “Fermionic quantum computation,” *Annals of Physics*, vol. 298, no. 1, pp. 210–226, May 2002, arXiv:quant-ph/0003137. [Online]. Available: <http://arxiv.org/abs/quant-ph/0003137>
- [8] M. Cerezo, G. Verdon, H.-Y. Huang, L. Cincio, and P. J. Coles, “Challenges and opportunities in quantum machine learning,” *Nature Computational Science*, vol. 2, no. 9, pp. 567–576, Sep. 2022, number: 9 Publisher: Nature Publishing Group. [Online]. Available: <https://www.nature.com/articles/s43588-022-00311-3>
- [9] J.-S. Chen, E. Nielsen, M. Ebert, V. Inlek, K. Wright, V. Chaplin, A. Maksymov, E. Páez, A. Poudel, P. Maunz, and J. Gamble, “Benchmarking a trapped-ion quantum computer with 29 algorithmic qubits,” Aug. 2023, arXiv:2308.05071 [quant-ph]. [Online]. Available: <http://arxiv.org/abs/2308.05071>
- [10] J. I. Cirac and P. Zoller, “Quantum computations with cold trapped ions,” *Phys. Rev. Lett.*, vol. 74, pp. 4091–4094, May 1995. [Online]. Available: <https://link.aps.org/doi/10.1103/PhysRevLett.74.4091>
- [11] A. Cowtan, S. Dilkes, R. Duncan, W. Simmons, and S. Sivarajah, “Phase gadget synthesis for shallow circuits,” *Electronic Proceedings in Theoretical Computer Science*, vol. 318, p. 213–228, May 2020. [Online]. Available: <http://dx.doi.org/10.4204/EPTCS.318.13>
- [12] A. W. Cross, L. S. Bishop, S. Sheldon, P. D. Nation, and J. M. Gambetta, “Validating quantum computers using randomized model circuits,” *Physical Review A*, vol. 100, no. 3, p. 032328, Sep. 2019, arXiv:1811.12926 [quant-ph]. [Online]. Available: <http://arxiv.org/abs/1811.12926>
- [13] M. G. Davis, E. Smith, A. Tudor, K. Sen, I. Siddiqi, and C. Iancu, “Towards optimal topology aware quantum circuit synthesis,” in *2020 IEEE International Conference on Quantum Computing and Engineering (QCE)*, 2020, pp. 223–234.



- [14] D. E. Deutsch and R. Penrose, “Quantum computational networks,” *Proceedings of the Royal Society of London. A. Mathematical and Physical Sciences*, vol. 425, no. 1868, pp. 73–90, Sep. 1989, publisher: Royal Society. [Online]. Available: <https://royalsocietypublishing.org/doi/10.1098/rspa.1989.0099>
- [15] C. Developers, “Cirq,” Jul. 2023. [Online]. Available: <https://doi.org/10.5281/zenodo.8161252>
- [16] B. Eastin and E. Knill, “Restrictions on transversal encoded quantum gate sets,” *Physical Review Letters*, vol. 102, no. 11, Mar. 2009. [Online]. Available: <http://dx.doi.org/10.1103/PhysRevLett.102.110502>
- [17] A. Erhard, J. J. Wallman, L. Postler, M. Meth, R. Stricker, E. A. Martinez, P. Schindler, T. Monz, J. Emerson, and R. Blatt, “Characterizing large-scale quantum computers via cycle benchmarking,” *Nature Communications*, vol. 10, no. 1, nov 2019. [Online]. Available: <https://doi.org/10.1038/s41467-019-13068-7>
- [18] E. Farhi, J. Goldstone, and S. Gutmann, “A Quantum Approximate Optimization Algorithm,” Nov. 2014, arXiv:1411.4028 [quant-ph]. [Online]. Available: <http://arxiv.org/abs/1411.4028>
- [19] D. Herman, C. Googin, X. Liu, A. Galda, I. Safro, Y. Sun, M. Pistoia, and Y. Alexeev, “A Survey of Quantum Computing for Finance,” Jun. 2022, arXiv:2201.02773 [quant-ph, q-fin]. [Online]. Available: <http://arxiv.org/abs/2201.02773>
- [20] P. Horodecki, M. Horodecki, and R. Horodecki, “General teleportation channel, singlet fraction and quasi-distillation,” Mar. 1999, arXiv:quant-ph/9807091. [Online]. Available: <http://arxiv.org/abs/quant-ph/9807091>
- [21] “IBM Quantum Experience,” <https://quantum-computing.ibm.com/>, accessed: 2020-11-15.
- [22] IonQ Staff, “IonQ Forte: The First Software-Configurable Quantum Computer.” [Online]. Available: <https://ionq.com/resources/ionq-forte-first-configurable-quantum-computer>
- [23] D. Jaksch, J. I. Cirac, P. Zoller, S. L. Rolston, R. Côté, and M. D. Lukin, “Fast quantum gates for neutral atoms,” *Phys. Rev. Lett.*, vol. 85, pp. 2208–2211, Sep 2000. [Online]. Available: <https://link.aps.org/doi/10.1103/PhysRevLett.85.2208>
- [24] Y. Kim, A. Eddins, S. Anand, K. X. Wei, E. van den Berg, S. Rosenblatt, H. Nayfeh, Y. Wu, M. Zaletel, K. Temme, and A. Kandala, “Evidence for the utility of quantum computing before fault tolerance,” *Nature*, vol. 618, no. 7965, pp. 500–505, Jun. 2023, number: 7965 Publisher: Nature Publishing Group. [Online]. Available: <https://www.nature.com/articles/s41586-023-06096-3>

- [25] E. Knill, D. Leibfried, R. Reichle, J. Britton, R. B. Blakestad, J. D. Jost, C. Langer, R. Ozeri, S. Seidelin, and D. J. Wineland, “Randomized Benchmarking of Quantum Gates,” *Physical Review A*, vol. 77, no. 1, p. 012307, Jan. 2008, arXiv:0707.0963 [quant-ph]. [Online]. Available: <http://arxiv.org/abs/0707.0963>
- [26] G. Li, Y. Ding, and Y. Xie, “Tackling the qubit mapping problem for nisq-era quantum devices,” 2019.
- [27] G. Li, A. Wu, Y. Shi, A. Javadi-Abhari, Y. Ding, and Y. Xie, “On the Co-Design of Quantum Software and Hardware,” in *Proceedings of the Eight Annual ACM International Conference on Nanoscale Computing and Communication*, ser. NANOCOM ’21. New York, NY, USA: Association for Computing Machinery, Sep. 2021, pp. 1–7. [Online]. Available: <https://dl.acm.org/doi/10.1145/3477206.3477464>
- [28] S. F. Lin, S. Sussman, C. Duckering, P. S. Mundada, J. M. Baker, R. S. Kumar, A. A. Houck, and F. T. Chong, “Let each quantum bit choose its basis gates,” in *2022 55th IEEE/ACM International Symposium on Microarchitecture (MICRO)*, 2022, pp. 1042–1058.
- [29] J. Liu, E. Younis, M. Weiden, P. Hovland, J. Kubiawicz, and C. Iancu, “Tackling the Qubit Mapping Problem with Permutation-Aware Synthesis,” May 2023, arXiv:2305.02939 [quant-ph]. [Online]. Available: <http://arxiv.org/abs/2305.02939>
- [30] E. Magesan, J. M. Gambetta, and J. Emerson, “Robust randomized benchmarking of quantum processes,” *Physical Review Letters*, vol. 106, no. 18, p. 180504, May 2011, arXiv:1009.3639 [quant-ph]. [Online]. Available: <http://arxiv.org/abs/1009.3639>
- [31] —, “Characterizing Quantum Gates via Randomized Benchmarking,” *Physical Review A*, vol. 85, no. 4, p. 042311, Apr. 2012, arXiv:1109.6887 [quant-ph]. [Online]. Available: <http://arxiv.org/abs/1109.6887>
- [32] A. Mandviwalla, K. Ohshiro, and B. Ji, “Implementing Grover’s Algorithm on the IBM Quantum Computers,” in *2018 IEEE International Conference on Big Data (Big Data)*, Dec. 2018, pp. 2531–2537. [Online]. Available: <https://ieeexplore.ieee.org/document/8622457>
- [33] J. R. McClean, I. D. Kivlichan, D. S. Steiger, Y. Cao, E. S. Fried, C. Gidney, T. Häner, V. Havlíček, Z. Jiang, M. Neeley, J. Romero, N. Rubin, N. P. D. Sawaya, K. Setia, S. Sim, W. Sun, K. Sung, and R. Babbush, “Openfermion: The electronic structure package for quantum computers,” 2017, cite arxiv:1710.07629. [Online]. Available: <http://arxiv.org/abs/1710.07629>
- [34] M. A. Nielsen, “A simple formula for the average gate fidelity of a quantum dynamical operation,” *Physics Letters A*, vol. 303, no. 4, pp.

- 249–252, oct 2002. [Online]. Available: <https://doi.org/10.1016%2Fs0375-9601%2802%2901272-0>
- [35] L. B. Oftelie, R. V. Beeumen, E. Younis, E. Smith, C. Iancu, and W. A. de Jong, “Constant-depth circuits for dynamic simulations of materials on quantum computers,” *Materials Theory*, vol. 6, no. 1, mar 2022. [Online]. Available: <https://doi.org/10.1186%2Fs41313-022-00043-x>
- [36] A. Peruzzo, J. McClean, P. Shadbolt, M.-H. Yung, X.-Q. Zhou, P. J. Love, A. Aspuru-Guzik, and J. L. O’Brien, “A variational eigenvalue solver on a quantum processor,” *Nature Communications*, vol. 5, no. 1, p. 4213, Jul. 2014, arXiv:1304.3061 [physics, physics:quant-ph]. [Online]. Available: <http://arxiv.org/abs/1304.3061>
- [37] Qiskit contributors, “Qiskit: An open-source framework for quantum computing,” 2023.
- [38] *Quantinuum System Model H2*, Quantinuum, 2023.
- [39] P. Rakyta and Z. Zimborás, “Efficient quantum gate decomposition via adaptive circuit compression,” 2022.
- [40] *Aspen-M-3 Quantum Processor*, Rigetti QCS, 2023.
- [41] H. Safi, K. Wintersperger, and W. Mauerer, “Influence of HW-SW-Co-Design on Quantum Computing Scalability,” Jun. 2023, arXiv:2306.04246 [quant-ph]. [Online]. Available: <http://arxiv.org/abs/2306.04246>
- [42] M. Sarovar, T. Proctor, K. Rudinger, K. Young, E. Nielsen, and R. Blume-Kohout, “Detecting crosstalk errors in quantum information processors,” *Quantum*, vol. 4, p. 321, Sep. 2020, arXiv: 1908.09855. [Online]. Available: <http://arxiv.org/abs/1908.09855>
- [43] D. Shin, H. Hübener, U. De Giovannini, H. Jin, A. Rubio, and N. Park, “Phonon-driven spin-Floquet magneto-valleytronics in MoS<sub>2</sub>,” *Nature Communications*, vol. 9, no. 1, p. 638, Feb. 2018, number: 1 Publisher: Nature Publishing Group. [Online]. Available: <https://www.nature.com/articles/s41467-018-02918-5>
- [44] S. Sivarajah, S. Dilkes, A. Cowtan, W. Simmons, A. Edgington, and R. Duncan, “t\$ket\$ : A Retargetable Compiler for NISQ Devices,” *Quantum Science and Technology*, vol. 6, no. 1, p. 014003, Jan. 2021, arXiv:2003.10611 [quant-ph]. [Online]. Available: <http://arxiv.org/abs/2003.10611>
- [45] R. R. Tucci, “An introduction to cartan’s kak decomposition for qc programmers,” 2005.

- [46] M. Weiden, E. Younis, J. Kalloor, J. Kubiatoicz, and C. Iancu, “Improving Quantum Circuit Synthesis with Machine Learning,” Jun. 2023, arXiv:2306.05622 [quant-ph]. [Online]. Available: <http://arxiv.org/abs/2306.05622>
- [47] S. Williams, A. Waterman, and D. Patterson, “Roofline: an insightful visual performance model for multicore architectures,” *Commun. ACM*, vol. 52, no. 4, p. 65–76, apr 2009. [Online]. Available: <https://doi.org/10.1145/1498765.1498785>
- [48] E. Younis and C. Iancu, “Quantum Circuit Optimization and Transpilation via Parameterized Circuit Instantiation,” Jun. 2022, arXiv:2206.07885 [quant-ph]. [Online]. Available: <http://arxiv.org/abs/2206.07885>
- [49] E. Younis, C. C. Iancu, W. Lavrijsen, M. Davis, E. Smith, and USDOE, “Berkeley quantum synthesis toolkit (bqskit) v1,” 4 2021. [Online]. Available: <https://www.osti.gov/servlets/purl/1785933>
- [50] J. Zhang, J. Vala, S. Sastry, and K. B. Whaley, “Minimum construction of two-qubit quantum operations,” *Physical Review Letters*, vol. 93, no. 2, p. 020502, Jul. 2004, arXiv:quant-ph/0312193. [Online]. Available: <http://arxiv.org/abs/quant-ph/0312193>